

# Exchange Engineering of a Two-Dimensional Half-Metal

Xin Liang Tan<sup>1,2,\*</sup>, Arthur Ernst<sup>3,4</sup>, Kenta Hagiwara<sup>1,2</sup>, Ying-Jiun Chen<sup>1,5</sup>,  
Claus Michael Schneider<sup>1,2,6</sup> and Christian Tuschke<sup>1,2,†</sup>

<sup>1</sup>*Peter Grünberg Institut (PGI-6), Forschungszentrum Jülich, Jülich 52425, Germany*

<sup>2</sup>*Fakultät für Physik, Universität Duisburg-Essen, Duisburg 47057, Germany*

<sup>3</sup>*Max-Planck-Institut für Mikrostrukturphysik, Weinberg 2, D-06120 Halle, Germany*

<sup>4</sup>*Institut für Theoretische Physik, Johannes Kepler Universität, A 4040 Linz, Austria*

<sup>5</sup>*Ernst Ruska-Centre for Microscopy and Spectroscopy With Electrons, Forschungszentrum Jülich, 52425 Jülich, Germany*

<sup>6</sup>*Department of Physics, University of California Davis, Davis, California 95616, USA*



(Received 23 December 2024; accepted 30 May 2025; published 16 July 2025)

We report the emergence of two-dimensional itinerant half-metallicity in a two-atomic-layer thick iron-palladium alloy. Against the common belief that spin-orbit coupling is adverse to half-metallicity, the complex interplay between exchange and spin-orbit coupling counterintuitively enables it via electronic band hybridization. The 2D ferromagnet is engineered directly via controlled alloying and is verified experimentally via spin-resolved band structure analyses. First-principles calculations corroborate its tunability by providing a systematic bottom-up approach through stepwise ground-state construction. The appearance of hybridization points at specific  $k$  points, via interplay between exchange and spin-orbit interactions, is responsible for the emergence of half-metallicity.

DOI: [10.1103/mx46-85zf](https://doi.org/10.1103/mx46-85zf)

The significance of the exchange interaction and spin-orbit coupling in solid-state physics, particularly for spin-related phenomena, is underscored by their foundational roles, serving as the cornerstone for the emergence of novel properties within materials. The exchange interaction, rooted in the Pauli exclusion principle, dictates the behavior of electron spins within a solid. The alignment of electron spins, driven by exchange interactions, gives rise to various magnetic states such as ferromagnetism and antiferromagnetism by breaking the time-reversal symmetry. Meanwhile, spin-orbit coupling, arising from relativistic effects on moving electrons in a potential, introduces a coupling between spin and orbital angular momenta, causing degeneracy lifting of electronic states. The combined influence of exchange interaction and spin-orbit coupling is a prime ingredient for the engineering of emergent electronic properties. A subclass among ferromagnets, the half metals are generally described as a spin current medium with a conducting majority spin channel

and an insulating minority spin channel. For this reason, half-metals are often hailed as the lynchpin in spintronics for their roles as spin filters and pure spin injection devices essential for spintronics applications such as spin transfer torque and spin-orbit torque devices.

Although substantial progress has been made on the theoretical front, where a plethora of half-metals are predicted, experimental evidence remains scarce. All known half-metals are of cryogenic temperature phases, making them impractical in technological applications [1]. Historically, the most well-known examples of half-metals are Heusler alloys and complex oxides. In reality, potential perturbations due to structural imperfections [2,3], surface, and interface effects [4,5] often lead to the breakdown of half-metallicity. For instance, the experiments on the prototypical half-metallic Heusler alloy NiMnSb [6,7] and magnetite Fe<sub>3</sub>O<sub>4</sub> [8,9] demonstrated large discrepancies in net spin-polarization due to the surface and bulk structural difference. Consequently, typical ferromagnets lose their high spin polarization and half-metallicity at their surface or when reduced to sub-nm thickness. Apart from recent theoretical predictions [10,11], there is no experimental evidence of a two-dimensional half-metal in existence. In addition to structural factors, the ubiquitous relativistic effect of spin-orbit coupling [12] and thermal depolarization mechanisms such as magnon and phonon excitations [13,14] are detrimental to the half-metallicity at finite temperatures. On the experimental front, a verification of half-metallicity is often limited because of challenges in spin resolutions of the electronic states [15,16].

\*Contact author: [xin.l.tan@ntnu.no](mailto:xin.l.tan@ntnu.no)

†Contact author: [c.tuschke@fz-juelich.de](mailto:c.tuschke@fz-juelich.de)

<sup>‡</sup>Present address: Center for Quantum Spintronics, Department of Physics, Norwegian University of Science and Technology, 7491 Trondheim, Norway.

Published by the American Physical Society under the terms of the [Creative Commons Attribution 4.0 International](https://creativecommons.org/licenses/by/4.0/) license. Further distribution of this work must maintain attribution to the author(s) and the published article's title, journal citation, and DOI.

This Letter presents a bottom-up optimization pathway for realizing a two-dimensional half-metallic film via direct band structure engineering. At the core of this endeavor lies the ambition to attain a fully polarized Fermi surface that is unattainable solely through exchange interaction. To circumvent this challenge, we leverage spin-orbit coupling to lift the band degeneracy at local  $k$  points, whereby a spin channel gap is leveled at the Fermi energy. In this pursuit, we employ two elemental ingredients: iron (Fe) and palladium (Pd). Fe, renowned for its large exchange, lays the foundation for robust magnetic interactions within the system. On the other hand, Pd is characterized by its susceptibility to polarization via the proximity effect and possesses significant spin-orbit coupling. Through systematic alloying and stoichiometry manipulation, we achieve a leveling of band hybridization points proximate to the Fermi energy, opening up a gap in one of the spin channels and, consequently, realizing a two-dimensional half-metallic film.

Depicted in Fig. 1(a), a well-established fabrication of ultrathin monolayers (ML) of the disordered FePd alloy on a Pd(001) single crystal was performed [17,18] using molecular beam epitaxy from a high-purity Fe rod, followed by mild annealing. The crystallinity and purity of the film and substrate were verified using low-energy electron diffraction and Auger electron spectroscopy [19]. In addition, the Fe to Pd composition of the film was tuned by controlling the nominal sub-ML Fe epitaxy in the deposition of the Fe thin films. In line with existing literature conventions [17,18], we utilized a mild annealing process on the Fe sub-MLs deposited on Pd(001) to induce alloying between interfacial layers, resulting in a two-monolayer thick FePd/Pd(001) structure, as illustrated in Fig. 1(a). Details of the fabrication of the ultrathin monolayers are provided in Fig. S4 of the Supplemental Material [19].

Our study employs the state-of-the-art spin-resolved momentum microscopy at the NanoESCA beamline [20] of the Elettra synchrotron in Trieste, Italy, to directly probe the spin-resolved electronic band structure of ultrathin FePd alloy monolayers on Pd(001). Spin-resolved momentum microscopy was carried out using a W(100) imaging spin filter [21]. The  $k$ -space mapping of the complete Brillouin zone with spin resolution permitted by momentum microscopy [22,23] permits the efficient optimization of the alloy composition crucial to the exchange engineering of the itinerant ferromagnetic film. All photoemission measurements were performed while keeping the sample at a temperature of 130 K, well below the Curie temperature of 370 K [18] of the FePd systems. The magnetic systems investigated in this study were remanently magnetized *in situ* at 130 K in the field-free microscope chamber in the  $-y$  direction before the measurements. In all measurements, the final energy resolution of the momentum microscope was set to  $< 50$  meV.

Figure 1(b) shows the spin-integrated Fermi surface of two-ML FePd/Pd(001) and bulk Pd(001). The stark

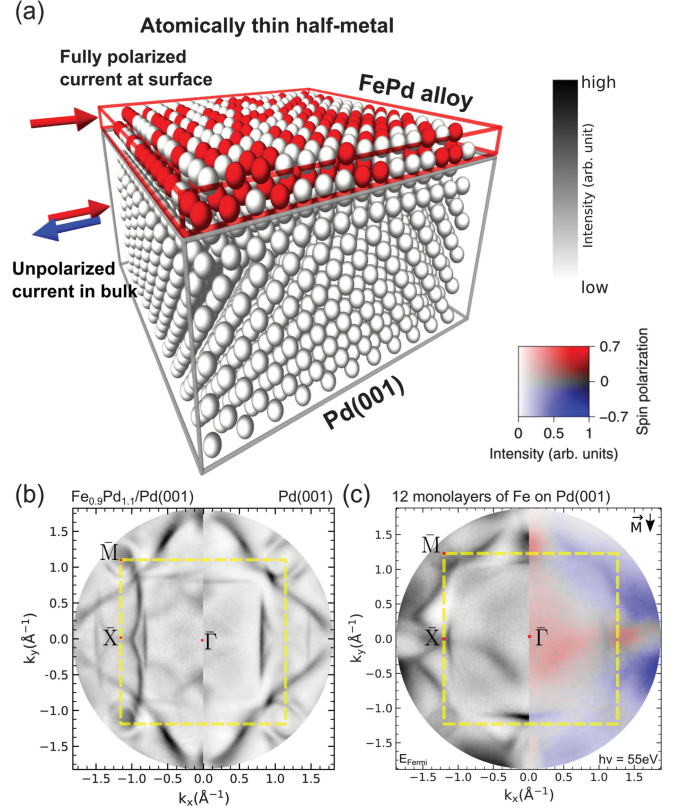


FIG. 1. (a) An illustration of a two-monolayer thick FePd alloy on Pd(001) showing the dimensionally confined half-metallic film. (b) The measured Fermi surface of two-ML thick FePd/Pd(001) (left half) and Pd(001) (right half). (c) The reference spin-integrated (left half) and spin-resolved (right half) Fermi surface of body-centered-cubic Fe represented in 12 ML Fe on Pd(001). Dashed yellow lines denote the surface Brillouin zone of a face-centered cubic lattice.

contrast between the Fermi surface of the disordered alloy monolayers and that of Pd(001) bulk states, particularly close to the Brillouin zone boundary, demonstrates a strong hybridization of states. Serving as a reference, the Fermi surface of a prototypical body-centered-cubic (bcc) Fe in the form of 12 ML of Fe on Pd(001) was measured using spin-resolved momentum microscopy along with its spin-integrated counterpart as shown in Fig. 1(c). Both the majority and minority spin channels of the ferromagnetic Fe were shown as the spin-up and spin-down bands, respectively, in line with the common textbook example of bulk bcc Fe states [24].

Spin-resolved momentum microscopy on two ML of FePd/Pd(001), in Fig. 2(a), revealed the hallmark feature of a half-metallic system with a fully spin-polarized Fermi surface. A negative energy (holelike) exchange-split spin-down band with a maximum at 175 meV below the Fermi energy is shown in the spin-resolved momentum map in Fig. 2(b). The spin-resolved experimental outcome demonstrated no significant spin-down states above the maximum of this band up to the Fermi level.

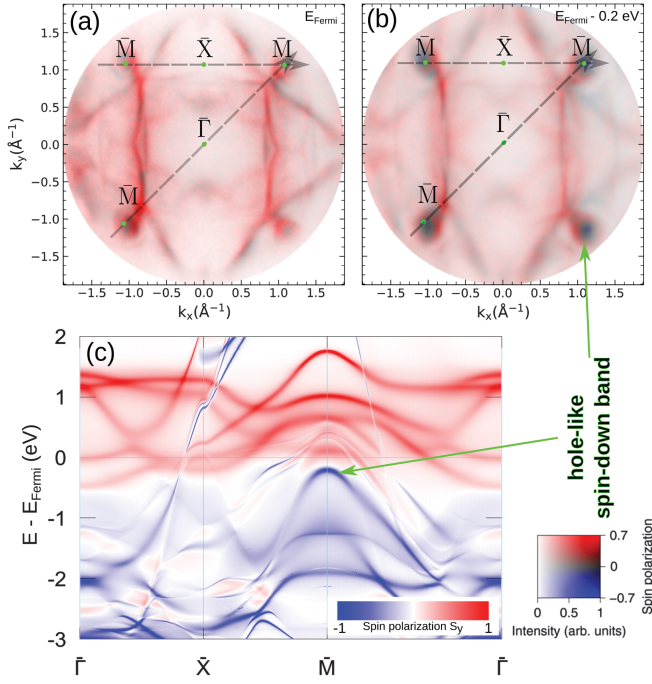


FIG. 2. Experimental spin-resolved (a) Fermi surface and (b) momentum map at 0.2 eV below the Fermi level of two-ML FePd/Pd(001). (c) Theoretical spin-resolved electronic structure of the topmost two surface layers of  $\text{Fe}_{0.9}\text{Pd}_{1.1}/\text{Pd}(001)$ . Green arrows denote the maximum of the holelike spin-down band centered at  $\bar{M}$ . The color scale in panel (c) represents the theoretical spin-resolved spectral function, while the two-dimensional color map corresponds to the experimentally measured spin polarization and photoemission intensity.

In concert with our experiment, layer- and spin-resolved calculations within the density functional theory are employed to understand the underlying physics. The calculations were performed using a Green function method within the multiple scattering theory, specially designed for semi-infinite systems such as surfaces and interfaces [25,26]. We utilized a generalized gradient approximation as the exchange-correlation functional [27] and used a coherent potential approximation [28–30] to account for the alloy’s chemical and structural compositions. First, we calculated bulk Pd in an fcc unit cell with the experimental lattice constant. Then, the self-consistently obtained potentials of Pd bulk were used to calculate the Green function of the host and Pd films deposited on the host. On top of the host, nine Pd and six vacuum layers were assembled and treated self-consistently within proper boundary conditions [31]. Figure 2(c) displays the theoretical spin-resolved Bloch spectral function from the first two surface layers of two ML of FePd/Pd(001) with 0.9 ML of nominal Fe [ $\text{Fe}_{0.9}\text{Pd}_{1.1}/\text{Pd}(001)$ ]. The theoretical calculations demonstrate good qualitative agreement with our experimental data as shown in Fig. S2 of the Supplemental Material [19]. Only the first two topmost layers of the thin film exhibit a near-ideal

half-metallic state. The spin-down band crosses the Fermi level around the  $\bar{M}$  point when the Bloch spectral function beyond the top two layers is integrated, inherently destroying its half-metallic property. Some discrepancies between theory and experiment can be explained by renormalization of the band structure due to electron-magnon interaction, which might be substantial in FePd alloys [18]. In addition, calculations of matrix elements within a photoemission model may improve agreement between theory and experiment. A juxtaposition of layer-resolved Fermi surfaces of two-ML FePd/Pd(001) [19] is shown in Fig. S1(a) of the Supplemental Material, while Fig. S1(b) of the Supplemental Material shows the evolution of the band structure with the increasing volume integration of the surface layers. Our theoretical calculations corroborated our surface-sensitive experiment, showing the confinement of the half-metallic electronic wave function to the top two layers of the system.

When the electronic interactions owing to the spin-orbit matrix are considered, the initially free electronlike bands depicted undergo band hybridization, ultimately resulting in the formation of a fully polarized Fermi surface as shown in Fig. 2(a) and in Fig. S1(a) of the Supplemental Material [19]. This emergence of a half-metallic Fermi surface can be understood as the electronic states of the same group representation being prohibited from crossing due to level repulsion in the Pauli exclusion principle. In contrast, the absence of spin-orbit coupling precludes the interaction between the spin-up majority and spin-down minority electronic bands. Consequently, a half-metallic electronic structure is not attainable, as shown in Fig. 3(a), as a significant contribution of the spin-down minority band crosses the Fermi level near the  $\bar{M}$  high-symmetry point of the surface Brillouin zone. Figure S2(a) of the Supplemental Material [19] shows the calculated fully relativistic spin-integrated electronic structure of  $\text{Fe}_{0.9}\text{Pd}_{1.1}/\text{Pd}(001)$ . Remarkably, the spin channel gap can be centered on the Fermi energy by precisely tuning the alloy to a composition of  $\text{Fe}_{0.9}\text{Pd}_{1.1}/\text{Pd}(001)$ .

At the heart of the half-metallicity lies the breaking of time-reversal symmetry due to magnetic ordering. A direct pathway for investigation is manipulating the nominal Fe content in the thin film, which effectively modulates the intralayer and interlayer exchange interactions [18]. A reduction in 0.2 ML of nominal Fe content from 0.9 ML to 0.7 ML of Fe, as shown in Figs. 3(b) and 3(c), culminated in a decrease in the exchange splitting by  $\sim 0.2 \text{ eV}$ . In addition to the exchange splitting control, the dissolution of half-metallicity in two MLs of FePd with nominal 0.7 MLs Fe ( $\text{Fe}_{0.7}\text{Pd}_{1.3}/\text{Pd}(001)$ ) in Figs. 3(b) and 3(c) demonstrates the strict parameter control on the nominal Fe MLs within the FePd alloy to realize the optimal condition for the half-metallic film. Meanwhile, an increase in 0.6 ML of the nominal Fe content, from 0.9 ML to 1.5 ML nominal Fe, results in an increase in



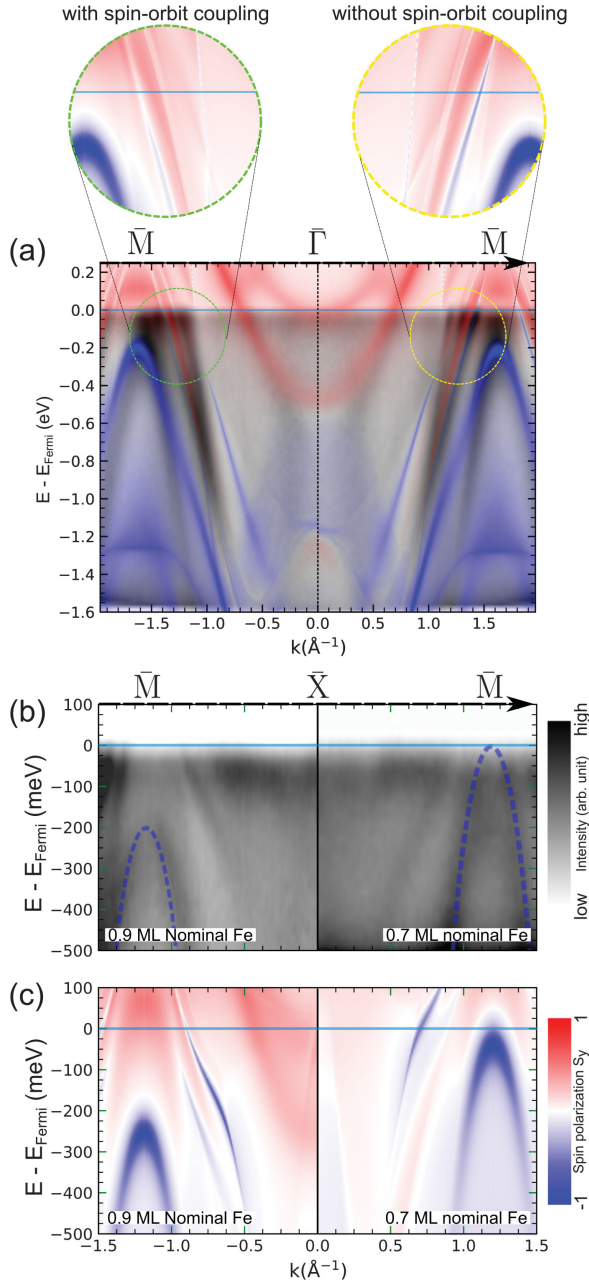


FIG. 3. (a) Experimental spin-integrated energy-momentum dispersion along  $\bar{M}-\bar{\Gamma}-\bar{M}$  high-symmetry points of two-ML FePd/Pd(001) with an overlay of calculated band structure with (left half) and without (right half) spin-orbit coupling. (b) Experimental spin-integrated energy-momentum dispersion along  $\bar{M}-\bar{X}-\bar{M}$  of  $\text{Fe}_{0.9}\text{Pd}_{1.1}/\text{Pd}(001)$  (left half) and  $\text{Fe}_{0.7}\text{Pd}_{1.3}/\text{Pd}(001)$  (right half) of 0.9 ML and 0.7 ML nominal Fe contents respectively. Blue dashed lines indicate the holelike spin-down bands. (c) Spin-resolved calculations along  $\bar{M}-\bar{X}-\bar{M}$  for the dispersions shown in (b). The dashed lines in Figs. 2(a) and 2(b) denote the momentum space from which the dispersions are extracted.

the exchange splitting at the  $\bar{M}$  point by  $\sim 0.6$  eV [19]. Figure S4 of the Supplemental Material [19] demonstrates that the magnitude of exchange splitting scales

proportionally by comparing the alloy thin films of different nominal Fe content. The spin-polarized electronic structure can be effectively engineered by balancing the exchange interaction and spin-orbit coupling. It is, however, important to note that due to the alloying nature of the monolayer fabrication, a lower Fe content will inevitably induce further inhomogeneity within the thin film; meanwhile, a higher Fe content is expected to induce structural phase transition and further disorder into the bulk [17,32].

On the other hand, the significant hybridization of the electronic states due to the proximity effect causes neighboring Pd atoms in the atomic layers to become spin polarized. As a result, the spin-up majority electronic state of polarized Pd is shifted to lower energies [18]. Figure S3 of the Supplemental Material [19] shows a systematic comparison of the theoretical electronic structures of a free-standing monolayer Fe in vacuum, one monolayer of pseudomorphic Fe on Pd(001), and  $\text{Fe}_{0.7}\text{Pd}_{1.3}/\text{Pd}(001)$ . Furthermore, Fig. S1 of the Supplemental Material [19] shows that the electronic bands of the topmost layer of the Pd substrate, namely the third layer, are spin polarized. Consequently, this results in an ultrathin half-metal with negative polarization, making it unique even among materials with negative spin polarization [33–35]. In other words, the spin current carried by the thin film is opposite to the direction of magnetization. This is evident in the comparison between the majority band (blue) of bcc Fe magnetized in the  $-y$  direction in Fig. 1(c), and the half-metallic Fermi surface of two ML FePd/Pd(001) in Fig. 2(a).

This study has highlighted an intuitive pathway to design a two-dimensional half-metallic system via the engineering of exchange interaction and spin-orbit coupling. The overall interplay between the exchange and the spin-orbit interaction can be tuned by varying the film's total ratio of Fe and Pd. We ultimately arrived at the optimal condition for half-metallicity in a two-elemental system and corroborated our results with first-principles calculations. Future studies may benefit from one-step photoemission calculations [36], which can account for matrix element effects and provide deeper insight into the orbital character of the bands [37] as well as the interplay between spin and orbital degrees of freedom in the electronic structure. The electronic structure of FePd alloys can be significantly affected by electron-magnon interaction [18,38], which can be accounted for in future studies.

For spintronic applications, such a system could be exploited readily as an ideal spin filter in thin films and heterostructures. Incidentally, this configuration also represents a prototypical setup for a spin-orbit torque system in which a ferromagnetic thin film is interfaced with a  $4d$  metal with significant spin-orbit coupling. An in-plane unpolarized current in the bulk Pd crystal, as shown in Fig. 1(a), can be used to magnetize or switch the spin polarization of the half-metallic film remanently. In a

nutshell, by employing state-of-the-art spin-resolved experiments and theoretical methods, our study suggests a reliable pathway for engineering electronic structures using fundamental interactions in physics, such as exchange and spin-orbit coupling. Our first-principles calculations demonstrated that  $\text{Fe}_{0.9}\text{Pd}_{1.1}/\text{Pd}(001)$  is an optimal condition for realizing two-dimensional half-metallicity.

**Acknowledgments**—A. E. acknowledges funding by the Fonds zur Förderung der wissenschaftlichen Forschung (FWF) under Grant No. I 5384 [Grant DOI: 10.55776/I5384].

**Data availability**—The data that support the findings of this Letter are not publicly available upon publication because it is not technically feasible and/or the cost of preparing, depositing, and hosting the data would be prohibitive within the terms of this research project. The data are available from the authors upon reasonable request.

- 
- [1] M. I. Katsnelson, V. Y. Irkhin, L. Chioncel, A. I. Lichtenstein, and R. A. de Groot, *Rev. Mod. Phys.* **80**, 315 (2008).
  - [2] H. Ebert and G. Schütz, *J. Appl. Phys.* **69**, 4627 (1991).
  - [3] S. Picozzi and A. J. Freeman, *J. Phys. Condens. Matter* **19**, 315215 (2007).
  - [4] I. Galanakis, *J. Phys. Condens. Matter* **14**, 6329 (2002).
  - [5] G. A. de Wijs and R. A. de Groot, *Phys. Rev. B* **64**, 020402(R) (2001).
  - [6] C. T. Tanaka, J. Nowak, and J. S. Moodera, *J. Appl. Phys.* **86**, 6239 (1999).
  - [7] R. J. Soulen, M. S. Osofsky, B. Nadgorny, T. Ambrose, P. Broussard, S. F. Cheng, J. Byers, C. T. Tanaka, J. Nowack, J. S. Moodera, G. Laprade, A. Barry, and M. D. Coey, *J. Appl. Phys.* **85**, 4589 (1999).
  - [8] S. Morton, G. Waddill, S. Kim, I. K. Schuller, S. Chambers, and J. Tobin, *Surf. Sci.* **513**, L451 (2002).
  - [9] J. de la Figuera and C. Tusche, *Appl. Surf. Sci.* **391**, 66 (2017).
  - [10] M. Ashton, D. Gluhovic, S. B. Sinnott, J. Guo, D. A. Stewart, and R. G. Hennig, *Nano Lett.* **17**, 5251 (2017).
  - [11] Q. Sun, J. Li, Y. Li, Z. Yang, and R. Wu, *Appl. Phys. Lett.* **119**, 062404 (2021).
  - [12] W. E. Pickett and H. Eschrig, *J. Phys. Condens. Matter* **19**, 315203 (2007).
  - [13] P. A. Dowben and R. Skomski, *J. Appl. Phys.* **95**, 7453 (2004).
  - [14] R. Skomski, *J. Phys. Condens. Matter* **19**, 315202 (2007).
  - [15] J. Kessler, *Polarized Electrons* (Springer, Berlin Heidelberg, 1976).
  - [16] M. Bode, *Rep. Prog. Phys.* **66**, 523 (2003).
  - [17] H. L. Meyerheim, R. Popescu, and J. Kirschner, *Phys. Rev. B* **73**, 245432 (2006).
  - [18] H. J. Qin, K. Zakeri, A. Ernst, L. M. Sandratskii, P. Buczek, A. Marmodoro, T. H. Chuang, Y. Zhang, and J. Kirschner, *Nat. Commun.* **6**, 6126 (2015).
  - [19] See Supplemental Material at <http://link.aps.org/supplemental/10.1103/mx46-85zf> for additional information on theoretical electronic structures on the layer-resolved KKR calculations and stoichiometrically related systems (2024).
  - [20] C. Wiemann, M. Patt, I. P. Krug, N. B. Weber, M. Escher, M. Merkel, and C. M. Schneider, *e-J. Surf. Sci. Nanotechnol.* **9**, 395 (2011).
  - [21] C. Tusche, M. Ellguth, A. Krasnyuk, A. Winkelmann, D. Kutnyakhov, P. Lushchik, K. Medjanik, G. Schönhense, and J. Kirschner, *Ultramicroscopy* **130**, 70 (2013).
  - [22] C. Tusche, A. Krasnyuk, and J. Kirschner, *Ultramicroscopy* **159**, 520 (2015).
  - [23] C. Tusche, Y.-J. Chen, C. M. Schneider, and J. Kirschner, *Ultramicroscopy* **206**, 112815 (2019).
  - [24] E. Młyńczak, I. Aguilera, P. Gospodarič, T. Heider, M. Jugovac, G. Zamborlini, J.-P. Hanke, C. Friedrich, Y. Mokrousov, C. Tusche, S. Suga, V. Feyer, S. Blügel, L. Plucinski, and C. M. Schneider, *Phys. Rev. B* **105**, 115135 (2022).
  - [25] M. Hoffmann, A. Ernst, W. Hergert, V. N. Antonov, W. A. Adeagbo, R. M. Geilhufe, and H. Ben Hamed, *Phys. Status Solidi (b)* **257** (2020).
  - [26] D. A. Rowlands, A. Ernst, B. L. Györfy, and J. B. Staunton, *Phys. Rev. B* **73**, 165122 (2006).
  - [27] J. P. Perdew, K. Burke, and M. Ernzerhof, *Phys. Rev. Lett.* **77**, 3865 (1996).
  - [28] P. Soven, *Phys. Rev.* **156**, 809 (1967).
  - [29] B. L. Györfy, *Phys. Rev. B* **5**, 2382 (1972).
  - [30] E. H. and H. Akai, *Int. J. Mod. Phys. B* **07**, 922 (1993).
  - [31] L. Szunyogh, B. Újfalussy, P. Weinberger, and J. Kollár, *Phys. Rev. B* **49**, 2721 (1994).
  - [32] S.-K. Lee, J.-S. Kim, B. Kim, Y. Cha, W. K. Han, H. G. Min, J. Seo, and S. C. Hong, *Phys. Rev. B* **65**, 014423 (2001).
  - [33] G. Hu and Y. Suzuki, *Phys. Rev. Lett.* **89**, 276601 (2002).
  - [34] C. Klewe, M. Meinert, J. Schmalhorst, and G. Reiss, *J. Phys. Condens. Matter* **25**, 076001 (2013).
  - [35] H. Suto, T. Nakatani, Y. Kota, N. Asam, H. Iwasaki, K. Amemiya, T. Mitsui, S. Sakai, S. Li, and Y. Sakuraba, *J. Magn. Magn. Mater.* **557**, 169474 (2022).
  - [36] J. Braun, J. Minár, and H. Ebert, *Phys. Rep.* **740**, 1 (2018).
  - [37] S. S. Brinkman, X. L. Tan, B. Brekke, A. C. Mathisen, O. Finnseth, R. J. Schenk, K. Hagiwara, M.-J. Huang, J. Buck, M. Kalläne, M. Hoesch, K. Rossnagel, K.-H. Ou Yang, M.-T. Lin, G.-J. Shu, Y.-J. Chen, C. Tusche, and H. Bentmann, *Phys. Rev. Lett.* **132**, 196402 (2024).
  - [38] S. Paischer, G. Vignale, M. I. Katsnelson, A. Ernst, and P. A. Buczek, *Phys. Rev. B* **107**, 134410 (2023).